Global agricultural N2O emission reduction strategies deliver climate benefits with minimal impact on stratospheric O3 recovery

npj | climate and atmospheric science

Article

Published in partnership with CECCR at King Abdulaziz University

https://doi.org/10.1038/s41612-024-00678-2

Global agricultural N_2O emission reduction strategies deliver climate benefits with minimal impact on stratospheric O_3 recovery

James Weber [1,5] ✉, James Keeble [2], Nathan Luke Abraham [3,4], David J. Beerling [1] & Maria Val Martin [1]

Agricultural nitrous oxide (N_2O) emission reduction strategies are required given the potency of N_2O as a greenhouse gas. However, the growing influence of N_2O on stratospheric ozone (O_3) with declining stratospheric chlorine means the wider atmospheric impact of N_2O reductions requires investigation. We calculate a N_2O emission reduction of 1.35 $TgN_2O\ yr^{-1}$ (~5% of 2020 emissions) using spatially separate deployment of nitrification inhibitors ($70–113 tCO_2e^{-1}) and crushed basalt (no-cost co-benefit) which also sequesters CO_2. In Earth System model simulations for 2025–2075 under high (SSP3-7.0) and low (SSP1-2.6) surface warming scenarios, this N_2O mitigation reduces NO_x-driven O_3 destruction, driving regional stratospheric O_3 increases but with minimal impact on total O_3 column recovery. By 2075, the radiative forcing of the combined N_2O and CO_2 reductions equates to a beneficial 9–11 ppm CO_2 removal. Our results support targeted agricultural N_2O emission reductions for helping nations reach net-zero without hindering O_3 recovery.

Nitrous oxide (N_2O) is the third most important anthropogenic greenhouse gas (GHG) after carbon dioxide (CO_2) and methane (CH_4)[1]. On a per molecule basis N_2O is ~273 times stronger than CO_2 and ~9 times stronger than CH_4 over a 100-year period (GWP_{100})[1]. Atmospheric mixing ratios of N_2O have risen from ~270 ppbv in the pre-industrial period to 332 ppbv in 2019, causing an effective radiative forcing of 0.21 ± 0.03 Wm^{-2}, about 10% of that from atmospheric CO_2 increases[1]. The rise in atmospheric N_2O has largely been driven by increases in human-induced emissions over the past 40 years, dominated by agricultural N_2O emissions[2–4], due to the use of N-fertilisers.

The potency of N_2O as a GHG has led to climate change and net-zero strategies recognising the importance of reducing N_2O emissions alongside CO_2 and CH_4[5,6]. Given the importance of the agricultural sector in the growth of N_2O emissions, there is an international focus on developing soil N_2O mitigation strategies, including nitrification inhibitors, biochar, and pH management[7,8].

N_2O is also an important stratospheric O_3-depleting substance[9] (Supplementary Eqs. 1, 2), and therefore N_2O emission reductions may be beneficial for both the recovery of stratospheric O_3 and from a global warming perspective[10–12]. However, the net effect of a sustained reduction in N_2O emissions is also dependent on the wider stratospheric evolution (e.g., changing temperatures driven by the particular GHG emission scenario). Chemical coupling between NO_x(=NO + NO_2) and other O_3-destroying chemical families (e.g., HO_x = H + OH + HO_2 and ClO_x = Cl+ClO; Supplementary Eqs 5 - 12. 3,4) could also be influential for O_3 destruction[11]. This coupling can change the balance between the active and less reactive reservoir forms for not only NO_x but also within the ClO_x and HO_x cycles and thus how much O_3 each can destroy. For example, increases in N_2O have been simulated to reduce ClO_x-driven O_3 destruction as more chlorine is sequestered into $ClONO_2$[11,13]. These factors complicate the prediction of the impact of N_2O emission reductions on O_3. Few studies have explored a sustained N_2O emission reduction within a chemistry-climate model simulation considering concurrent changes to other influential species (e.g., CFCs) across multiple future stratospheric climate scenarios.

Here, we investigate the impact of an N_2O emissions reduction (~5% of present-day global total emissions and ~25% of direct agriculture emissions)

[1]Leverhulme Centre for Climate Change Mitigation, School of Biosciences, University of Sheffield, Sheffield S10 2TN, UK. [2]Lancaster Environment Centre, Lancaster University, Lancaster, UK. [3]Centre for Atmospheric Science, Yusuf Hamied Department of Chemistry, University of Cambridge, Cambridge CB2 1EW, UK. [4]National Centre for Atmospheric Science, Yusuf Hamied Department of Chemistry, University of Cambridge, Cambridge CB2 1EW, UK. [5]Present address: Department of Meteorology, University of Reading, Reading RG6 6ET, UK. ✉e-mail: j.m.weber@reading.ac.uk

from the spatially separate application of basalt and nitrification inhibitors to agricultural land, on stratospheric O_3 over the next 50 years (Methods). These two approaches are emerging strategies for reducing N_2O emissions from agricultural soils: application of nitrification inhibitors is a straightforward technique while amending soils with crushed basalt which undergoes chemical weathering in the soil profile increases pH, thus acting in a similar manner to liming[14–18]. Additional benefits of amending soils with crushed basalt, a technique known as enhanced rock weathering (ERW), include CO_2 sequestration and improved soil health[14,19]. Combined, these techniques are projected to reduce N_2O emissions by 1.35 $TgN_2O\ yr^{-1}$ (Fig. 1a, b) which corresponds to a reduction of 0.37 $GtCO_2e\ yr^{-1}$ (based on a GWP_{100} of 273).

We use the state-of-the-art Earth System model, UKESM1, with fully interactive tropospheric and stratospheric chemistry[20,21] to simulate the effects of N_2O reductions across two stratospheric futures, SSP3-7.0 (high tropospheric warming, greater stratospheric cooling) and SSP1-2.6 (lower tropospheric warming, lower stratospheric cooling), which are both Montreal Protocol-compliant. The different tropospheric and stratospheric conditions in SSP3-7.0 and SSP1-2.6 arise from their diverging emission pathways for GHGs (Supplementary Fig. 1) and other climate forcers and can influence stratospheric O_3. This allows for a comprehensive examination of the effect of implementing an N_2O emission reduction plan across a wide window of future trajectories to broaden the applicability of the results. The temporal evolution of the lower boundary condition (LBC) of N_2O in UKESM1 (effectively N_2O's surface concentration) is lowered to simulate the sustained emission reduction of 1.35 Tg $N_2O\ yr^{-1}$ (Fig. 1(c); Methods). This adjustment is performed in simulations where all other conditions (e.g., CO_2, CH_4, other well-mixed GHG concentrations and anthropogenic and biomass burning emissions) follow the relevant SSP scenario.

To isolate the impact of N_2O emission reductions, we compare the output from the simulations with lowered N_2O LBC, denoted SSP370_low_N2O and SSP126_low_N2O (Table 1), to the respective SSP3-7.0 and SSP1-2.6 simulations performed for the ScenarioMIP part of CMIP6[22], denoted SSP370 and SSP126 respectively. Comparison between the control and low_N2O scenarios are referred to in terms of the background scenario (e.g., "SSP370 comparison" refers to SSP370_low_N2O vs SSP370). Since the ScenarioMIP SSP370 and SSP126 simulations did not output the key stratospheric O_3 loss fluxes, a single simulation was performed using the same conditions as SSP370 and SSP126 with these fluxes output and denoted SSP370_flux and SSP126_flux, respectively (Table 1). We present first the impact of N_2O emission reductions on N_2O concentrations, then on stratospheric O_3 (identifying the drivers of the changes where possible) and wider stratospheric composition, total column O_3 (TCO) and finally the associated radiative forcing from N_2O, CO_2 and O_3 changes. We consider the TCO change over the full 2025-2075 period and zonal changes in O_3 in particular detail for the periods 2040-2050 and 2065-2075 to examine the progressive reduction in stratospheric chlorine (Fig. 1d) and in build-up of the difference in N_2O between the control and low_N2O scenarios (Fig. 1c).

Results

Zonal mean changes in N_2O and O_3

The reductions in the N_2O LBC applied to simulate the 1.35 $TgN_2O\ yr^{-1}$ decrease in N_2O emissions from agricultural sources (Methods) lead to

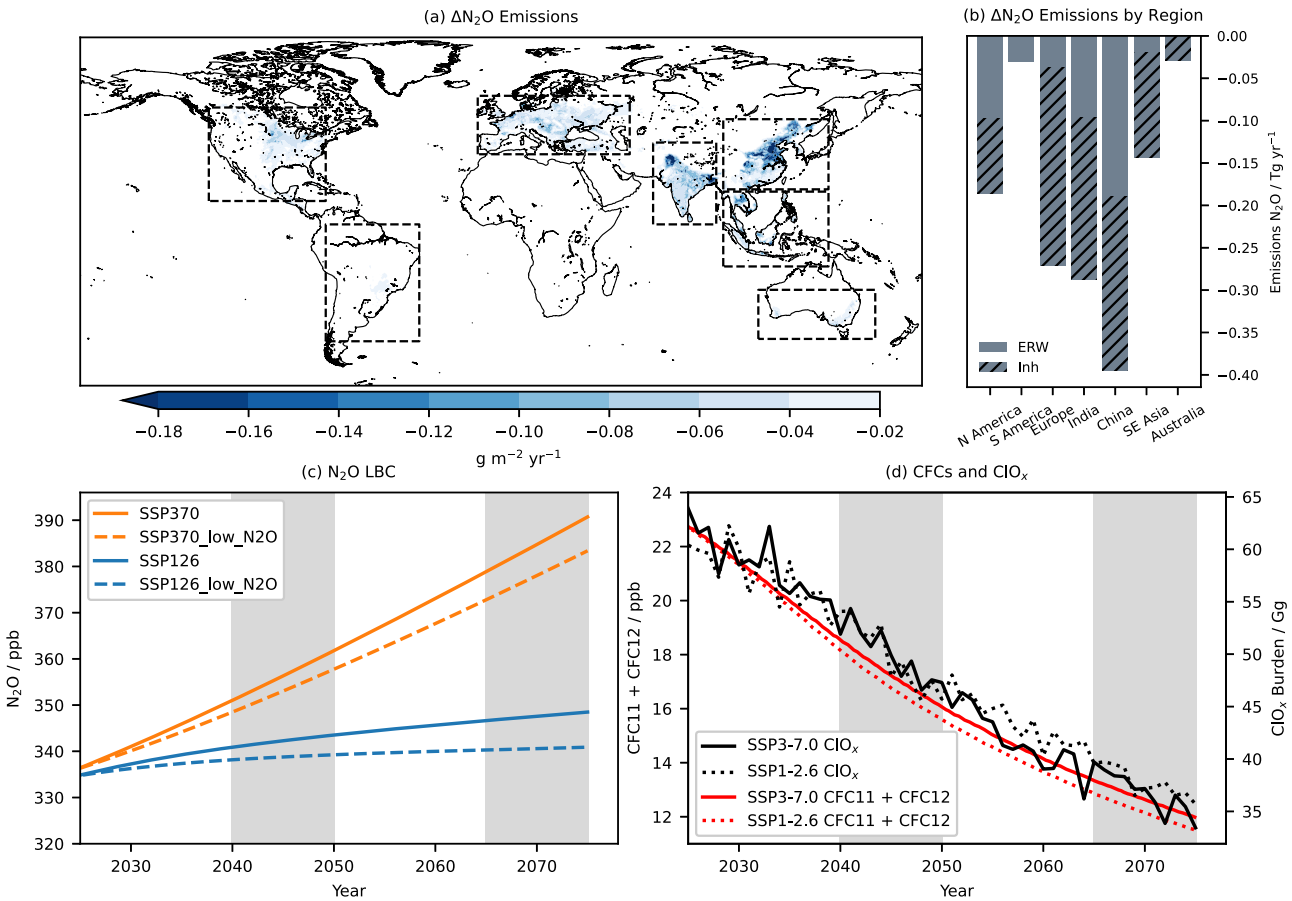

Fig. 1 | N_2O Emission Changes,LBCs and Chlorinated Species. a Change in N_2O emissions from the application of basalt and nitrogen inhibitors and **b** change in emissions by regions shown by dashed lines in **a** from enhanced rock weathering (ERW) and inhibitor (Inh) contributions. **c** Control and perturbed N_2O lower boundary conditions used in SSP126/SSP370 and SSP126_low_N2O /SSP370_low_N2O simulations. **d** Sum of major CFCs (CFC11 and CFC12) global mean mixing ratio and ClO_x(=Cl + ClO) burden in SSP126 and SSP370. Shaded regions in (**c**,**d**) show periods of particular focus.

decreases in low altitude concentrations which propagate vertically as N_2O enters the stratosphere and is destroyed by photolysis and reaction with $O(^1D)$[11]. These reductions exceed 5 ppb throughout the low and mid-stratosphere (2065-2075 mean) in both SSP scenarios, with attendant reductions in total reactive nitrogen (NO_y, Supplementary Fig. 2).

In both low_N2O scenarios, there are increased annual mean stratospheric O_3 mixing ratios relative to their respective base SSP scenario around 5-20 hPa across mid-latitudes and tropics (Fig. 2). This increase persists throughout all seasons (Supplementary Figs. 3–6), with statistical significance (95% confidence) observed on an annual basis only in the SSP370_low_N2O vs. SSP370 comparison, where the increase exceeds 100 ppb (~1-1.5%, Supplementary Fig. 7) in 2065–2075. Under both SSP370 and SSP126 conditions, the O_3 increase is more pronounced in 2065–2075 than in 2040–2050, reflecting the greater reduction in N_2O (see NO_x as the main driver of O_3 change). The spatial change in tropical and mid-latitude O_3 in Fig. 2 is largely replicated when the trend in ozone difference from 2025-2075 is also considered (Supplementary Fig. 8).

Table 1 | UKESM1 simulations

Scenario (no. of ensemble members)	N_2O LBCs	Background conditions***
SSP126* (16)	Base SSP1-2.6	SSP1-2.6
SSP126_flux** (1)		
SSP126_low_N2O (3)	Lowered SSP1-2.6 (2025-2075)	
SSP370* (15)	Base SSP3-7.0	SSP3-7.0
SSP370_flux** (1)		
SSP370_low_N2O (3)	Lowered SSP3-7.0 (2025-2075)	

*Performed for ScenarioMIP.
** Copy of one ScenarioMIP ensemble member run for 2040-2050 and 2065-2075 to generate control reaction fluxes in this study.
*** CO_2, CH_4 and other well-mixed GHG LBCs, anthropogenic and biomass burning emissions, crop and pasture fraction, nitrogen deposition.

Additionally, increased annual mean O_3 mixing ratios are modelled throughout the northern hemisphere (NH) polar stratosphere for 2040-2050 in the SSP126_low_N2O relative to the SSP126 scenario. This increase is most pronounced during wintertime (DJF; Supplementary Fig. 3). In contrast, for the 2065-2075 period, decreased annual mean ozone mixing ratios are simulated in the same region, with the largest changes also occurring in DJF. However, we note that neither of these changes are statistically significant at the 95% confidence level. These variations likely reflect the large, dynamically induced variability observed in stratospheric ozone over the Arctic (e.g.[23–27],), rather than a direct response to changes in N_2O.

NO_x as the main driver of O_3 change

To investigate the chemical processes driving the differences in O_3 between the control and low_N2O runs shown in Fig. 2, we first examine changes to the $NO_2 + O$ flux, as this is the O_3 loss flux most closely linked to the N_2O changes explored in this study. Then, we follow this analysis by considering changes in the O_3 loss from the ClO_x and HO_x catalytic cycles. Specifically, we compare the fluxes of the catalytic O_3 loss reactions in the three low_N2O runs (e.g., SSP370_low_N2O) to those in the single control run with reaction fluxes (e.g., SSP370_flux), since the other control runs did not have reaction fluxes output. To assess if the single control run is representative of the wider control ensemble (e.g., SSP370), we compare in Fig. 3 the zonal mean O_3 change between the low_N2O and single control (e.g., SSP370_low_N2O vs. SSP370_flux) and the low_N2O and full ensemble member comparisons (e.g. SSP370_low_N2O vs. SSP370), denoting these as the "single" and "full" comparisons, respectively. In cases where the O_3 change is consistent in sign and magnitude between the "single" and "full" comparisons, we propose the attribution of O_3 changes based on the flux differences in the "single" comparison also applies to the "full" comparison.

The clearest example is the SH mid-latitude O_3 increase evident in both the SSP370_low_N2O vs. SSP370 (Fig. 3a) and SSP370_low_N2O vs. SSP370_flux (Fig. 3b) comparisons at altitudes of around 5–20 hPa for the 2065-2075 period. Examining the SSP370_low_N2O vs. SSP370_flux case in more detail, the area of increased ozone mixing ratios, along with neighbouring O_3 decreases, shows spatial anticorrelation with changes in NO_x-driven O_3 destruction, specifically the flux of $NO_2 + O$ (Fig. 3c). This

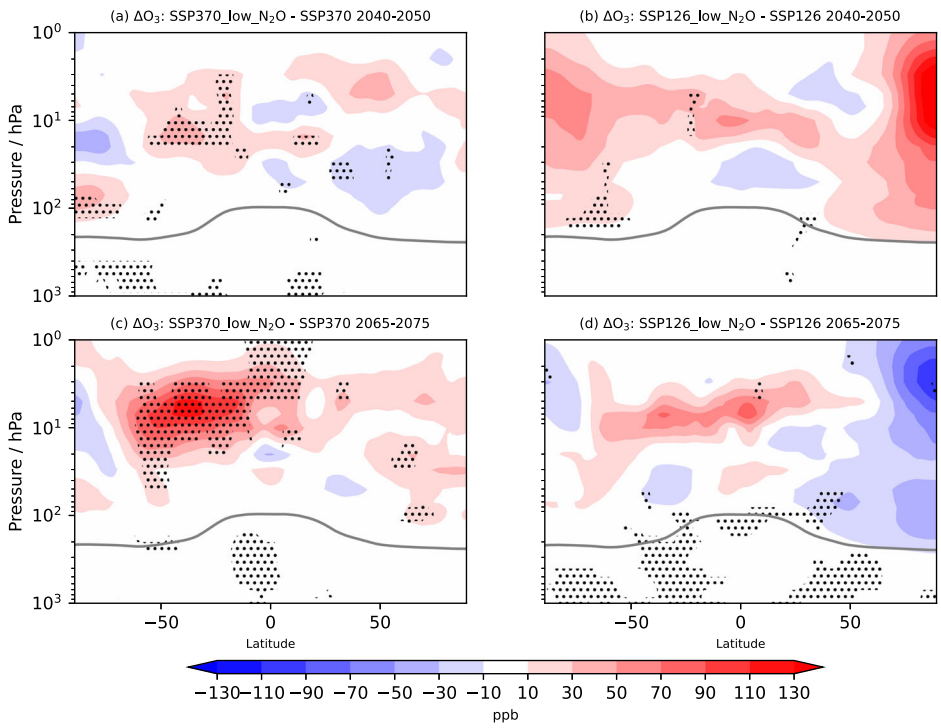

Fig. 2 | O_3 Changes. Zonal mean change in O_3 mixing ratio averaged over 2040-2050 for **a** SSP370_low_N2O - SSP370 and **b** SSP126_low_N2O - SSP126 and 2065-2075 for **c** SSP370_low_N2O - SSP370 and **d** SSP126_low_N2O - SSP126. Stippling shows regions of statistical significance (95% confidence) and the grey line show s mean tropopause location.

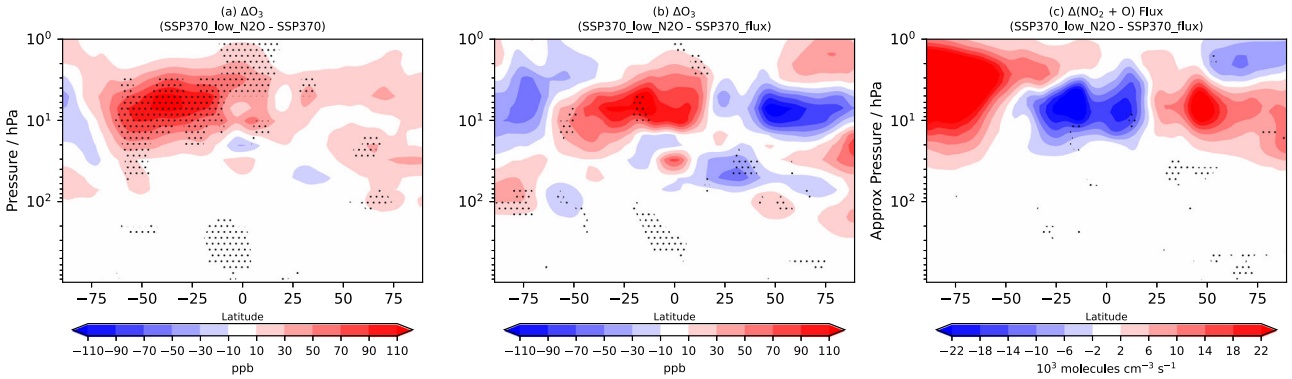

Fig. 3 | Changes to O_3 and NO_x-driven O_3 Loss. Zonal mean change in annual mean O_3 between **a** SSP370_low_N2O and SSP370 (same as 2c), **b** SSP370_low_N2O and SSP370_flux and **c** annual mean change in $NO_2 + O$ flux between SSP370_low_N2O and SSP370_flux. Stippling shows regions of statistical significance (95% confidence).

Fig. 4 | TCO and radiative forcing. a TCO timeseries for control and low_N2O simulations. TCO timeseries for 75-90 S for October (lowest historical TCO) for **b** SSP370 and SSP370_low_N2O and **c** SSP126 and SSP126_low_N2O. Shading in **a**–**c** shows standard deviation and values in square brackets show regression slope ± error (95% confidence). **d** Radiative forcing from changes to N_2O and CO_2 (from ERW's associated 2 $GtCO_2$ yr^{-1} CDR) in 2050 and 2075. Text on bars shows change in CO_2 concentrations (in ppm) required to achieve the same radiative forcing.

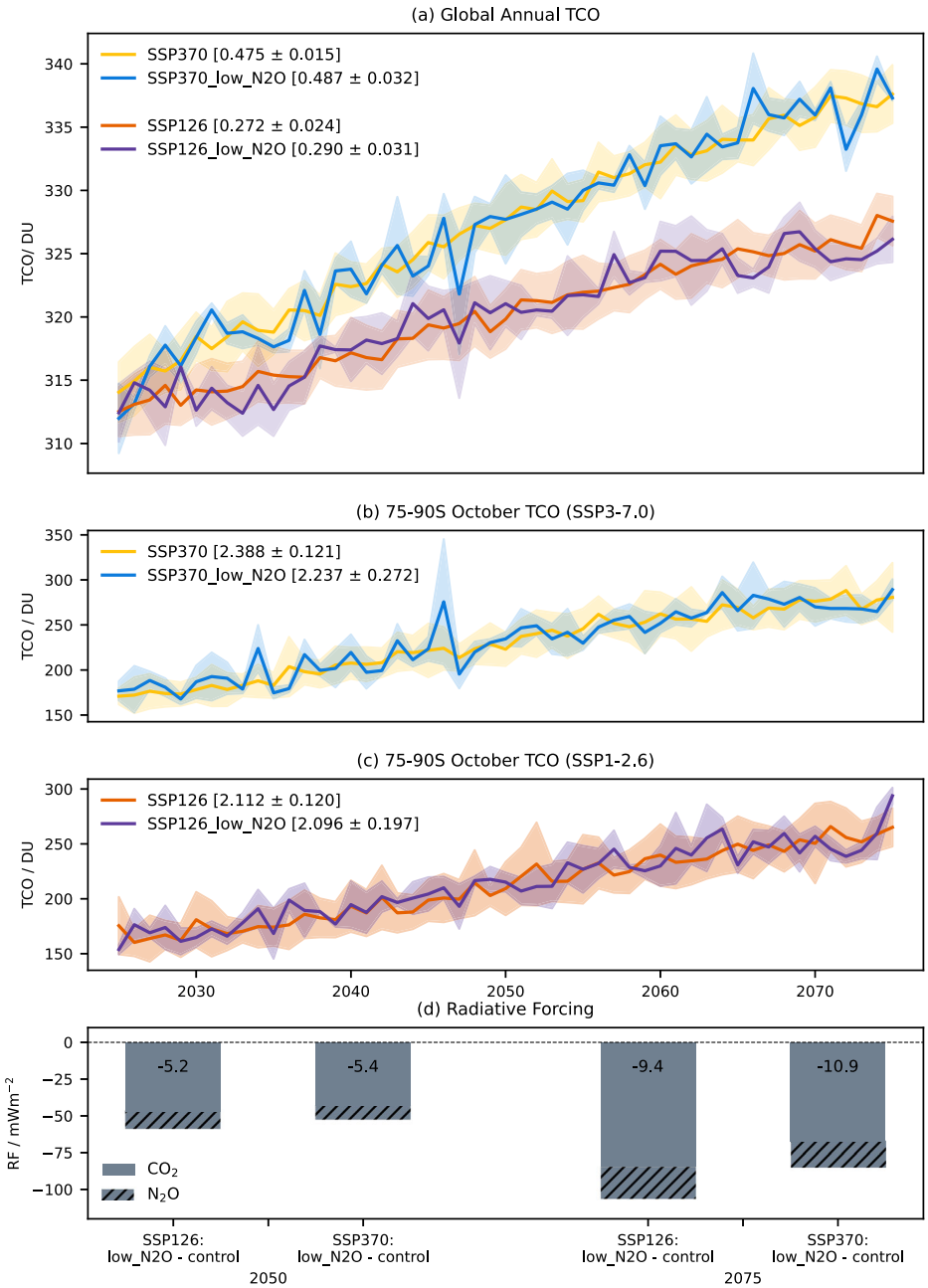

provides evidence that these local ozone changes represent a direct response to changes in NO_x-driven loss and thus N_2O. While the consistency of mid-latitude O_3 changes in the full and single comparisons is weaker on an annual basis for 2040–2050 (Supplementary Fig. 9), there is greater consistency on a seasonal level (e.g., MAM; Supplementary Fig. 10), with spatial anticorrelation persisting between O_3 changes and NO_x-driven O_3 destruction.

For the SSP126 scenarios, mid-latitude O_3 changes also exhibit consistency between the full (SSP126_low_N2O vs. SSP126) and single (SSP126_low_N2O vs. SSP126_flux) comparisons in 2065-2075, particularly during DJF and MAM, and display anticorrelation with NO_x-driven O_3 destruction changes (Supplementary Fig. 11). By contrast, mid-latitude O_3 changes are less consistent between the full and single comparisons for SSP126 at 2040-2050, even on a seasonal basis, hindering attribution.

The increase of O_3 in response to reduced N_2O is in line with prior studies[28,29] which simulated reductions to stratospheric O_3 following increases to future N_2O concentrations. While this study only employs a single model (UKESM1), the robustness of our results is supported by reference to studies where UKESM1 (or its atmospheric chemistry and aerosols component, UKCA) was compared to other chemistry-climate models running the same experiments designed to examine the impact of changing N_2O on stratospheric O_3. Specifically, O_3 in the lower and mid-stratosphere (Fig. 2) showed similar sensitivity to changes in surface N_2O in UKCA and most of the models involved in the CCMI project[30] and AerChemMIP[31].

We next consider the impact of NO_x changes to the ClO_x (Supplementary Eqs. 5, 6) and HO_x (Supplementary Eqs. 7–10) catalytic cycles via chemical coupling (Supplementary Eqs. 3, 4). We find the anti-correlation between changes in O_3 and ClO_x-driven O_3 destruction (specifically ClO + O) is weak (Supplementary Fig. 12). There is some anti-correlation between changes in O_3 and HO_x-driven O_3 destruction ($HO_2 + O$ and $HO_2 + O_3$; Supplementary Fig. 13) under SSP1-2.6 conditions, but this mostly occurs in regions where the change in O_3 is not consistent between the "full" and "single" comparisons (Supplementary Fig. 10), making assessment of this signal's robustness difficult. Overall, our findings suggest the impact of cross-family coupling (i.e. changes in NO_x driving changes in ClO_x or HO_x and thus O_3) is small relative to impact of direct changes to NO_x-driven O_3 loss. This small impact is consistent with prior studies which identified these interactions as having small significant effects; for example Meul et al.[15] found that interactions between chlorine and N_2O and methane products increased O_3 by 2.5% (relative to simulations where coupling was prevented).

For the SSP126 northern high latitude O_3 changes (Fig. 2b, d), consistency is observed between the SSP126_low_N2O vs. SSP126 and SSP126_low_N2O vs. SSP126_flux comparisons, particularly for DJF. However, attributing the drivers presents a challenge. Neither NO_x- nor ClO_x-driven O_3 destruction correlates well with changes to O_3. As stated above, polar regions exhibit greater dynamical variability, and the fact that the NH high latitude O_3 changes are dominated by winter (DJF) changes, suggests these statistically non-significant changes are unlikely to be a direct response to changes in N_2O emissions.

Wider atmospheric chemistry response

N_2O can affect the HO_x and ClO_x cycles by perturbing the partitioning between their active and reservoir species (Supplementary Eqs. 3, 4). Although we find the effect of this cross-family coupling on O_3 is limited, we extend our analysis to examine the response of wider atmospheric composition. This includes the families involved in catalytic O_3-destruction (ClO_x, NO_x and HO_x) and the reservoir species ($ClONO_2$ and $HONO_2$), all of which are considered in our simulations. Having already identified a lack of clear coupling between NO_x and ClO_x/HO_x in the context of O_3 destruction (Supplementary Figs. 9, 10), we find the changes in the global vertical profiles of NO_x, ClO_x, HO_x, and $ClONO_2$ below 2% and nearly all fall within ±1 standard deviation (σ) of the control ensemble mean (Supplementary Figs. 12, 13). Changes in HNO_3 exceed 1 σ, but remain below 2%. This small signal relative to the control ensemble is consistent at both poles (75–90 latitude) in winter and summer, with only HNO_3 regularly exceeding 1 σ from the control ensemble mean (Supplementary Figs. 14, 15). Overall, this suggests the N_2O emissions reduction considered here is unlikely to alter wider stratospheric composition, with the background climate scenario (i.e. SSP) exerting a more pronounced influence.

Total column O_3 response to N_2O mitigation

Previously, we considered vertically resolved stratospheric O_3 changes in response to reductions in N_2O emissions. When considering the impact of N_2O mitigation on O_3 recovery, we must consider total column O_3 (TCO, the amount of O_3 in a vertical column from the surface to the edge of space) as well, since this is often used to evaluate future projections of O_3 recovery (e.g., O_3 return dates are calculated using TCO values[32]. This is also important from a human health perspective as TCO has a direct relation to the attenuation of harmful ultraviolet solar radiation. Although we report local, and in some instances statistically significant, changes in stratospheric O_3 concentrations (Fig. 2), there are no significant differences between the control and low_N2O scenarios for TCO on a global annual basis (Fig. 4a) or in the high latitude band 75–90 S in October (historically the period and region with lowest TCO) (Fig. 4b, c). Future TCO projections are more dependent on the wider climate scenario than N_2O mitigation. The greater stratospheric cooling (Supplementary Fig. 16) (which increases O_3 as the odd-oxygen loss reaction in the Chapman cycle slows; Supplementary Eqs. 13–16[28]) and higher tropospheric O_3 burden seen in SSP3-7.0 projections contribute to higher TCO values in this scenario when compared to SSP1-2.6[32].

The time evolution of the TCO difference between the control and low_N2O simulations also displays no clear trend when decomposed latitudinally (Supplementary Fig. 17). At high northern latitudes, several periods during 2040–2050 exhibit anomalously large TCO increases in SSP126_low_N2O relative to SSP126, while this trend is reversed for 2065–2075, in line with the zonal mean changes in Fig. 2b, d) which we attribute to dynamical variability.

Radiative impact of N_2O, CO_2 and O_3 changes

The reduction in N_2O emissions from agricultural lands, and attendant lower atmospheric N_2O concentrations, leads to a radiative forcing of −10 (−18) and −12 (−22) mWm^{-2} at 2050 (2075) relative to the contemporaneous SSP370 and SSP126 controls (Methods). The values at 2075 are equivalent in magnitude to 11% and 13% of the multi-model pre-industrial to present day forcing from N_2O increases[33]. Despite exhibiting very similar reductions in global mean N_2O concentrations, the associated forcing is smaller in the SSP370 case. This is primarily because CO_2 and CH_4, whose absorption of LW outgoing radiation partially overlaps with that of N_2O, are present at higher concentrations in SSP370 than SSP126. The predicted net 2 Gt CO_2 yr^{-1} removal by ERW[19] from the basalt application to croplands considered here yields atmospheric CO_2 concentrations which are 4.3 (8.6) and 4.1 (7.4) ppm lower at 2050 (2075) than those of the SSP370 and SSP126 controls, respectively (Methods). Combined, these relatively modest changes are equivalent to reductions of 10.9 ppm for SSP370 and 9.4 ppm for SSP126, approximately 4% and 22% of the respective increases in CO_2 over 2025–2075 (Fig. 4d).

O_3 itself also acts as a GHG but is most potent in the mid and upper troposphere and much weaker in the stratosphere[34] where most of the change occurs in this study. While stratospheric O_3 changes can affect tropospheric O_3 via stratosphere-troposphere exchange and photolysis, we do not find a robust radiative forcing from O_3 changes under either scenario or time period (Supplementary Fig. 18; Methods).

Discussion

The stratospheric O_3 layer is critically important to protecting life on Earth from harmful ultraviolet radiation. Consequently, any climate change mitigation strategy which could perturb it must be rigorously evaluated. Nitrous oxide is an important stratospheric O_3 depleting substance in the

21st Century[10,11], thus emission abatement strategies, critical to limiting anthropogenic warming, warrant detailed investigation from an O_3 perspective.

Our simulation of N_2O emissions reductions over five decades within two climatic futures captures the effect of concurrent changes to N_2O and other important variables. Our findings suggest the TCO recovery is protected, both globally and at high latitudes, with modest, and in places statistically significant, O_3 increases in mid-latitude stratospheric regions likely driven by reductions in NO_x-driven O_3 destruction. Although the wider stratospheric conditions complicate the influence of N_2O on stratospheric O_3, we capture these effects in our Earth System model simulation experiments. Increasing concentrations of atmospheric CO_2 will cool the stratosphere due to the radiative balance between the heating from solar radiation absorption by O_3 and the cooling from the emission of infra-red radiation from CO_2 (and H_2O). This CO_2-driven stratospheric cooling, combined with higher CH_4 concentrations which drive greater HO_x concentrations, is more pronounced in the scenarios with greater tropospheric warming (e.g., SSP3-7.0) than with lower warming (e.g., SSP1-2.6). Consequently, this dual effect reduces the efficiency of the NO_x-driven O_3 destruction. In contrast, the long-term decline of stratospheric chlorine following the Montreal Protocol has the opposite effect, increasing the efficiency of N_2O in destroying O_3 as less NO_x is sequestered into its less reactive reservoir forms[35]. However, the minimal impact on TCO is consistent in both climate scenarios, suggesting such N_2O emission abatement strategies would not hinder the existing, carefully planned international policies that facilitate O_3 recovery (e.g., the Montreal Protocol) under a broad window of atmospheric composition and climate futures.

Furthermore, there are substantial climatic and ecological co-benefits from efforts to curb agricultural N_2O emissions. Reducing N_2O emissions yields lower atmospheric concentrations, thus providing a climatic benefit (i.e., negative radiative forcing relative to the control). This reinforces the importance of reducing emissions identified in multiple net zero and climate change mitigation plans (e.g.[6,36,37]). The application of nitrification inhibitors can reduce nitrate leaching into water courses and natural habitats (e.g.[38,39]), and therefore, reduce the negative impacts of excessive nitrogen burdens on ecosystems and human health.

We highlight an important economic distinction between N_2O mitigation strategies considered here. For ERW practices involving amending agricultural soils with crushed basalt for CO_2 removal purposes, N_2O mitigation (0.47 $TgN_2O\ yr^{-1}$) is a cost-free co-benefit[18]. When converted to CO_2 equivalents, N_2O emissions reductions from ERW (*19*; Table 1) reduce abatement costs by between 2.3% (North America) and 9% (China). In contrast, the application of nitrification inhibitors to farmland incurs specific additional costs. Application at \$28–45 ha^{-1} [40] to the 600 Mha of agriculture soils considered in this study for nitrification inhibitors (Methods) would cost \$17–27 billion annually. The associated abatement (0.87 $TgN_2O\ yr^{-1}$) corresponds to \$70–113/tCO_2e.

Unlike CO_2 emissions, which are projected to reach net-zero by 2035–2070 for scenarios with 1.5 °C warming, emissions of CH_4 and N_2O are predicted to remain positive given the challenges of complete abatement[41]. The use of nitrogen fertilisers and manure in agriculture constitutes the largest anthropogenic source of N_2O, making both practices the focus of mitigation via agricultural practices and policies in efforts to reach net-zero[40]. Such policies include, for example, incentivised targeting of increased cropland N-use efficiency (i.e., increasing yields with the same amount of N input)[42]. Our analysis of possible worldwide efforts to deliver sustained reductions in agricultural N_2O emissions for five decades in two diverging future climatic scenarios (SSP3-7.0 and SSP1-2.6) suggests such efforts will not disrupt TCO recovery. The benefit of ERW is it delivers a cost saving of \$8.5–\$13 billion a year for comparable N_2O reductions obtained with nitrification inhibitors. Our analyses further emphasise the importance of N_2O mitigation for delivering co-benefits for climate and sustainable agriculture (with no additional costs in the case of ERW), and thus the requirement for urgent exploration of the wide-scale deployment of N_2O mitigation schemes. This will be particularly important in future decades as the drive to reach net-zero emissions, and pressures to increase food production to feed a rising human population, intensify.

Methods

Agriculture soil N_2O emission reduction

To develop a mitigation scenario for direct agricultural soil N_2O emissions, we used the agriculture emissions from the global N_2O multimodel intercomparison project (NMIP[43]). This dataset was derived from seven process-based terrestrial biosphere models in natural and crop ecosystems and formed the basis of the IPCC 2021 soil N_2O budget estimates[44]. As a baseline, we used the averaged direct N_2O emissions from nitrogen additions in the agricultural sector from all seven models in 2010–16, with a spatial distribution of 50 × 50 km horizontal resolution and monthly temporal resolution.

For abatement strategies, we considered enhanced rock weathering (ERW) and fertilizer nitrification inhibitors. Following Val Martin et al.[15], we implemented ERW by considering the impact of basalt amendments in croplands on soil N_2O emissions. This involved a reduction in soil N_2O emissions resulting from increases in soil pH from basalt amendments, strategically applied across five main agricultural regions (North America, Brazil, Europe, India, and China) to achieve a targeted removal of 2 $GtCO_2yr^{-1}$ [19]. This resulted in a reduction of direct agriculture soil N_2O from 5.19 to 4.69 $TgN_2O\ yr^{-1}$ with basalt applied across 400 Mha of cropland soils.

For fertiliser nitrification inhibitors, we implemented this strategy in agriculture grid cells without ERW, considering a 50% reduction in soil N_2O emissions (ref. 40; *8*). Given the high cost of fertiliser nitrification inhibitors (28-45 \$ ha^{-1}; [40]), application was limited to agricultural regions in countries in the global north. This strategy was applied to about 600 Mha of agriculture soils, leading to a further reduction of total soil N_2O crop emissions from 4.69 to 3.84 $TgN_2O\ yr^{-1}$.

The integration of these two mitigation strategies yielded a substantial N_2O reduction of 1.35 $TgN_2O\ yr^{-1}$, constituting about 40% reduction in our primary agricultural regions and a 25% reduction in global direct agricultural N_2O emissions. This approach reflects a moderate nitrogen regulation scenario, strategically focusing on specific countries and agricultural areas while considering economic feasibility. The spatial distribution of the changes in soil agriculture N_2O emissions is illustrated in Fig. 1(a).

UKESM1 model setup

All simulations were conducted using the fully coupled configuration of UKESM1.0[20], with a horizontal resolution of 1.25° × 1.9° with 85 vertical levels up to 85 km, as used in CMIP6. This setup considers all aspects of the Earth System, including the atmosphere, land surface, ocean, and cryosphere, and allows them to interact.

The atmosphere is simulated with fully interactive stratospheric and tropospheric chemistry[21] and the GLOMAP-mode aerosol scheme, which simulates sulfate, sea-salt, black carbon, organic matter, and dust but not currently nitrate aerosol[45]. While a nitrate scheme is now available in UKESM[46], it was not available for CMIP6 and, as the runs performed for this study used the same model version as those done specifically for CMIP6, nitrate aerosol was not used here either.

Emissions of well-mixed greenhouse gases, including N_2O, CH_4, and CO_2, were not explicitly simulated; rather lower boundary conditions (LBC) were applied which evolved over time to represent the concentrations assumed by the SSP1-2.6 and SSP3-7.0 pathways[47]. The LBCs of N_2O were adjusted as described below.

Anthropogenic and biomass burning time series emissions, nitrogen deposition, and crop and pasture fraction constraints for the appropriate scenario were supplied as input.

UKESM1 simulations

This study considered four scenarios, including standard SSP3-7.0 and SSP1-2.6 alongside two perturbed scenarios, SSP370_low_N2O and SSP126_low_N2O (Table 1). The perturbed scenarios are identical to their corresponding SSP, but consider an adjusted lower boundary condition

(LBC) of N_2O to simulate an annual emission reduction of 1.35 $TgN_2O\ yr^{-1}$ (Fig. 1c) (see LBC Adjustment).

Simulations SSP370_flux and SSP126_flux, identical to the control SSP3-7.0 and SSP1-2.6 but with the inclusion of important reaction flux diagnostics, were also performed.

All simulations used the same UKESM1 model version and setup as the UKESM1 simulations performed for ScenarioMIP, to ensure comparability.

We compared model output from 16/15 ensemble members for both SSP1-2.6 and SSP3-7.0 performed in UKESM1 for ScenarioMIP to output from three ensemble members each for SSP370_low_N2O and SSP126_low_N2O. The SSP370_low_N2O and SSP126_low_N2O were initialised at 2025 from three different members of the corresponding base SSP at 2025 and run for 51 years (2025-2075 inclusive).

To increase confidence in our findings, we chose to perform simulations of three ensemble members with a sustained emission reduction of 1.35 $TgN_2O\ yr^{-1}$, considering the computational expense and variability of fully coupled simulations.

All simulations used a fully-coupled setup with interactive ocean and land surface, with the land surface constrained only by SSP-specific crop and pasture fractions for each grid cell. SSP-specific time-dependent LBCs of other well-mixed greenhouse gases (CO_2, CH_4, CFC12, and HFC134a), nitrogen deposition, and anthropogenic and biomass burnings from Input4MIPs remained consistent across all simulations based on the same SSP. For example, SSP370 and SSP370_low_N2O had the same LBC time series for CH_4 and anthropogenic and biomass-burning emissions, differing only in their N_2O LBC.

Reaction fluxes were calculated online during the model runs and output as total flux through a reaction in moles per second for each grid cell. Fluxes were divided by grid cell volume to normalise for the varying cell volume and allow for comparison of flux between different regions of the atmosphere (e.g. Fig. 3).

LBC Adjustment

To ensure comparability with the simulations performed for ScenarioMIP (where N_2O concentrations were controlled using LBCs rather than emissions), the reduction of N_2O emissions here was implemented by altering N_2O LBC.

Total simulated N_2O emissions for SSP3-7.0 and SSP1-2.6 were first extracted from Meinshausen et al.[47] where anthropogenic emissions are time-dependent (Fig. 2 in [47]) and natural emissions are fixed over time. The concentration of N_2O can be expressed as in Eq. 1.

$$\frac{dN_2O}{dt} = E(t) - \frac{N_2O}{\tau(N_2O)} \quad (1)$$

where E(t) are the time-dependent N_2O emissions and the lifetime of N_2O, $\tau(N_2O)$, is a function of N_2O concentration (Eq. 2) (Meinshausen et al.[47]).

$$\tau(N_2O) = 139\left(\frac{C^t_{N2O}}{C^0_{N2O}}\right)^{-0.04} \quad (2)$$

where C^0_{N2O} and C^t_{N2O} are mixing ratios of N_2O in the pre-industrial period (273 ppbv) and the time of interest, respectively.

To calculate the impact of the emission reduction, E(t) is reduced by 1.35 $TgN_2O\ yr^{-1}$, and Eq. 1 solved to yield a new N_2O mixing ratio. Finally, these mixing ratios are scaled by 1.033 to reflect the fact that the N_2O LBC value in UKESM1 is consistently 3.3 ± 0.1% higher than the global mean N_2O concentrations for both SSP3-7.0 and SSP1-2.6 up to 2100.

FAIR Simulation for atmospheric CO_2 estimates

To estimate the effect of a sustained 2 $GtCO_2\ yr^{-1}$ removal on atmospheric CO_2 mixing ratio, we used the FAIR model v2.1.0[48] with the AR6 calibration (https://zenodo.org/record/7545157#.Y85wwC-l30o; last accessed 24th Jan 2023).

We conducted four simulations: control SSP3-7.0 and SSP1-2.6 simulations, and perturbed simulations identical to the respective control, except that from 2025 onward, CO_2 emissions were lowered by 2 $GtCO_2\ yr^{-1}$. For example, the perturbed SSP3-7.0 simulation had identical forcing and emissions as the control SSP3-7.0, except that at 2025, its CO_2 emissions were reduced by 2 $GtCO_2\ yr^{-1}$.

These simulations were run with every configuration of FAIR to span assessment of the IPCC AR6 (ECS best estimate 3 °C, 5–95% range 2 °C–5 °C) along with several other assessed ranges from the IPCC AR6 including historical warming, transient climate response, and aerosol radiative forcing. The average difference in atmospheric CO_2 concentration between the respective control and perturbed simulations at 2075 was then considered as the impact of the sustained 2 $GtCO_2\ yr^{-1}$ removal.

Radiative forcing calculations

The radiative forcing from changes to N_2O and CO_2 were estimated using the radiative kernel from Etminan et al.[49] with scenario- and time-appropriate background concentrations.

The radiative forcing from changes to O_3 was calculated by taking the difference between the mean control O_3 field (e.g. SSP370 at 2040-2050) and mean low_N2O O_3 field (e.g. SSP370_low_N2O at 2040-2050) and applying this to the radiative kernel of Rap et al.[50]) updated for the whole atmosphere as described in Iglesias-Suarez et al.[51].

Data availability

Model output from simulations performed for this study is freely available on the Zenodo repository https://doi.org/10.5281/zenodo.10401772 with accompanying explanatory documentation. Output from model simulations performed for CMIP6 are available on the Earth System Grid Federation website and can be downloaded from there (https://esgf-index1.ceda.ac.uk/search/cmip6-ceda/, ESGF, last accessed 10th January 2024).

Code availability

Input emissions from SSP3-7.0 and SSP1-2.6 are available from the input4MIPs repository (https://esgf-node.llnl.gov/projects/input4mips/) maintained by ESGF. Due to intellectual property right restrictions, we cannot provide either the source code or documentation papers for the Unified Model/UKESM. The Met Office Unified Model/UKESM is available for use under licence. For further information on how to apply for a licence, see https://www.metoffice.gov.uk/research/approach/modelling-systems/unified-model (last accessed 1st August 2023). Suite numbers for the runs are listed in the README which accompanies the UKESM1 data repository on Zenodo.

Received: 22 January 2024; Accepted: 29 May 2024;
Published online: 07 June 2024

References

1. Forster, P. T. et al. The Earth's Energy Budget, Climate Feedbacks, and Climate Sensitivity. In Climate Change 2021: The Physical Science Basis. Contribution of Working Group I to the Sixth Assessment Report of the Intergovernmental Panel on Climate Change (Cambridge University Press, 2021).
2. Thompson, R. L. et al. Acceleration of global N_2O emissions seen from two decades of atmospheric inversion. *Nat. Clim. Chang.* **9**, 993–998 (2019).
3. Tian, H. et al. A comprehensive quantification of global nitrous oxide sources and sinks. *Nature* **586**, 248–256 (2020).
4. Tian, H. et al. Global nitrous oxide budget 1980–2020. Preprint at https://doi.org/10.5194/essd-2023-401 (2023).
5. Nisbet, E. G. et al. Atmospheric methane and nitrous oxide: Challenges along the path to Net Zero. *Philos. Trans. R. Soc. A* **379**, 20200457 (2021).
6. Climate Change Act (2008) https://www.legislation.gov.uk/ukpga/2008/27/contents (last accessed 14th November 2023).

7. Eory, V. et al. Non-CO_2 abatement in the UK agricultural sector by 2050. Summary report submitted to support the 6th carbon budget in the UK December 2020 https://www.theccc.org.uk/wp-content/uploads/2020/12/Non-CO2-abatement-in-the-UK-agricultural-sector-by-2050-Scottish-Rural-College.pdf, (last accessed 20th November 2023).
8. Grados, D. et al. Synthesizing the evidence of nitrous oxide mitigation practices in agroecosystems. *Environ. Res. Lett.* **17**, 114024 (2020).
9. Solomon, S. Stratospheric ozone depletion: a review of concepts and history. *Review of Geophysics* **37**, 275–316 (1999).
10. Ravishankara, A. R. et al. Nitrous oxide (N_2O): The dominant ozone-depleting substance emitted in the 21st century. *Science* **326**, 123–125 (2009).
11. Portmann, R. W., Daniel, J. S. & Ravishankara, A. R. Stratospheric ozone depletion due to nitrous oxide: influences of other gases. *Philos. Trans. R. Soc. B* **367**, 1256–1264 (2012).
12. Revell, L. E., Bodeker, G. E., Huck, P. E., Williamson, B. E. & Rozanov, E. The sensitivity of stratospheric ozone changes through the 21st century to N_2O and CH_4. *Atmos. Chem. Phys.* **12**, 11309–11317 (2012).
13. Meul, S., Oberländer-Hayn, S., Abalichin, J. & Langematz, U. Nonlinear response of modelled stratospheric ozone to changes in greenhouse gases and ozone depleting substances in the recent past. *Atmos. Chem. Phys.* **15**, 6897–6911 (2015).
14. Beerling, D. J. et al. Farming with crops and rocks to address global climate, food and soil security. *Nat. Plants* **4**, 138–147 (2018).
15. Val Martin, M. et al. Improving nitrogen cycling in a land surface model (CLM5) to quantify soil N_2O, NO, and NH_3 emissions from enhanced rock weathering with croplands. *Geosci. Model Dev.* **16**, 5783–5801 (2023).
16. Blanc-Betes, E. et al. In silico assessment of the potential of basalt amendments to reduce N2O emissions from bioenergy crops. *GCB Bioenergy* **13**, 224–241 (2021).
17. Kantzas, E. P. et al. Substantial carbon drawdown potential from enhanced rock weathering in the United Kingdom. *Nat. Geosci.* **15**, 382–389 (2022).
18. Chiaravalloti, I. et al. Mitigation of soil nitrous oxide emissions during maize production with basalt amendments. *Frontiers in Climate* **5**, 1203043 (2023).
19. Beerling, D. J. et al. Potential for large-scale CO_2 removal via enhanced rock weathering with croplands. *Nature* **583**, 242–248 (2020).
20. Sellar, A. et al. UKESM1: Description and Evaluation of the U.K. Earth System Model. *Journal of Advances in Modeling Earth System* **11**, 4513–4558 (2019).
21. Archibald, A. T. et al. Description and evaluation of the UKCA stratosphere–troposphere chemistry scheme (StratTrop vn 1.0) implemented in UKESM1. *Geoscientific Model Dev* **13**, 1223–1266 (2020).
22. O'Neill, B. et al. The Scenario Model Intercomparison Project (ScenarioMIP) for CMIP6. *Geosci. Model Dev* **9**, 3461–3482 (2016).
23. World Meteorological Organization (WMO), Scientific Assessment of Ozone Depletion: 2022, GAW Report No. 278, 509, WMO, Geneva, (2022).
24. Strahan, S. E., Douglass, A. R. & Steenrod, S. D. Chemical and dynamical impacts of stratospheric sudden warmings on Arctic ozone variability. *J. Geophys. Res. Atmos.* **121**, 11, 836–11,851 (2016).
25. Weber, M. et al. The Brewer-Dobson circulation and total ozone from seasonal to decadal time scales. *Atmos. Chem. Phys.* **11**, 11221–11235 (2011).
26. Tegtmeier, S., Rex, M., Wohltmann, I. & Kruger, K. Relative importance of dynamical and chemical contributions to Arctic wintertime ozone. *Geophys. Res. Lett.* **35**, L17801 (2008).
27. Randel, W. J., Wu, F. & Stolarski, R. Changes in column ozone correlated with the stratospheric EP flux. *J. Meteorol. Soc. Jpn.* **80**, 849–886 (2002).
28. Fleming, E. L., Jackman, C. H., Stolarski, R. S. & Douglass, A. R. A model study of the impact of source gas changes on the stratosphere for 1850–2100. *Atmos. Chem. Phys.* **11**, 8515–8541 (2011).
29. Stolarski, R. S., Douglass, A. R., Oman, L. D. & Waugh, D. W. Impact of future nitrous oxide and carbon dioxide emissions on the stratospheric ozone layer. *Environ. Res. Lett.* **10**, 034011 (2015).
30. Morgenstern, O. et al. Ozone sensitivity to varying greenhouse gases and ozone-depleting substances in CCMI-1 simulations. *Atmos. Chem. Phys.* **18**, 1091–1114 (2018).
31. Zeng, G. et al. Attribution of stratospheric and tropospheric ozone changes between 1850 and 2014 in CMIP6. *models. J. Geophys. Res*. **127**, e2022JD036452 (2022).
32. Keeble, J. et al. Evaluating stratospheric ozone and water vapour changes in CMIP6 models from 1850 to 2100. *Atmos. Chem. Phys.* **21**, 5015–5061 (2021).
33. Thornhill, G. D. et al. Effective radiative forcing from emissions of reactive gases and aerosols – a multi-model comparison. *Atmos. Chem. Phys.* **21**, 853–874 (2021).
34. Lacis, A. A., Wuebbles, D. J. & Logan, J. A. Radiative forcing of climate by changes in the vertical distribution of ozone. *J. Geophys. Res.: Atmospheres* **95**, 9971–9981 (1990).
35. Revell, L. E. et al. The effectiveness of N_2O in depleting stratospheric ozone. *Geophys. Res. Lett.* **39**, L15806 (2012).
36. U.S. Department of States, The long-term strategy of the United States: pathways to net-zero greenhouse gas emissions by 2050. U.S. Department of State and U.S. Exec. Off. President, Washington DC, pp.1–65 (2021).
37. European Comission, Directorate for Climate Action, EU Emissions Trading System (EU ETS), https://climate.ec.europa.eu/eu-action/eu-emissions-trading-system-eu-ets_en (last access April 25, 2024).
38. Cui, M. et al. Effective mitigation of nitrate leaching and nitrous oxide emissions in intensive vegetable production systems using a nitrification inhibitor, dicyandiamide. *J. Soils Sediments* **11**, 722–730 (2011).
39. Gao D. et al. 2021 IOP Conf. Ser.: Earth Environ. Sci. 690 012012.
40. MacLeod, M. et al. Cost-Effectiveness of Greenhouse Gas Mitigation Measures for Agriculture: A Literature Review, OECD Food, Agriculture and Fisheries Papers, No. 89, OECD Publishing, Paris (2015).
41. Riahi, K. R. et al. Mitigation pathways compatible with long-term goals. In IPCC, 2022: Climate Change 2022: Mitigation of Climate Change. Contribution of Working Group III to the Sixth Assessment Report of the Intergovernmental Panel on Climate Change (Cambridge University Press, 2022).
42. Kanter, D. R. et al. Improving the social cost of nitrous oxide. *Nat. Clim. Chang* **11**, 1008–1010 (2021).
43. Tian, H. et al. The global N2O model intercomparison project. *BAMS* **99**, 1231–1251 (2018).
44. Canadell, J. G. et al: Global Carbon and other Biogeochemical Cycles and Feedbacks. In Climate Change 2021: The Physical Science Basis. Contribution of Working Group I to the Sixth Assessment Report of the Intergovernmental Panel on Climate Change.(Cambridge University Press, 2021).
45. Mulcahy, J. P. et al. Description and evaluation of aerosol in UKESM1 and HadGEM3-GC3.1 CMIP6 historical simulations. *Geosci. Model Dev.* **13**, 6383–6423 (2020).
46. Jones, A. C. et al. Exploring the sensitivity of atmospheric nitrate concentrations to nitric acid uptake rate using the Met Office's Unified Model. *Atmos. Chem. Phys.* **21**, 15901–15927 (2021).
47. Meinshausen, M. et al. The shared socio-economic pathway (SSP) greenhouse gas concentrations and their extensions to 2500. *Geosci. Model Dev.* **13**, 3571–3605 (2020).
48. Leach, N. et al. FaIRv2.0.0: a generalized impulse response model for climate uncertainty and future scenario exploration. *Geosci. Model Dev.* **14**, 3007–3036 (2021).

49. Etminan, M. et al. Radiative forcing of carbon dioxide, methane, and nitrous oxide: A significant revision of the methane radiative forcing. *Geophys. Res. Lett* **43**, 24 (2016).
50. Rap, A. et al. Satellite constraint on the tropospheric ozone radiative effect. *Geophys. Res. Lett.* **42**, 5074–5081 (2015).
51. Iglesias-Suarez, F. et al. Key drivers of ozone change and its radiative forcing over the 21st century. *Atmos. Chem. Phys.* **18**, 6121–6139 (2018).

Acknowledgements

This work was supported by the UKRI Future Leaders Fellowship Programme awarded to Maria Val Martin (MR/T019867/1) and the Leverhulme Research Centre Award (RC-2015–02) to David J. Beerling. This work used Monsoon2, a collaborative high-performance computing facility funded by the Met Office and the Natural Environment Research Council, the ARCHER2 UK National Supercomputing Service, and JASMIN, the UK collaborative data analysis facility. We also thank Isabella Chiaravalloti and Noah Planavsky for useful comments in an initial draft of the manuscript.

Author contributions

J.W., M.V.M., and D.J.B. conceived the study. M.V.M. calculated changes in N_2O emissions from nitrification inhibitor application and ERW scenario. J.W. set up and performed simulations with advice from N.L.A. J.W. performed the analysis with advice from J.K., M.V.M., and D.J.B. J.W. drafted the manuscript with input from M.V.M. and D.J.B. All authors reviewed and commented on the manuscript.

Competing interests

D.J.B. has a minority equity stake in companies (Future Forest/Undo), is a member of the Advisory Board of The Carbon Community, a UK carbon removal charity, and the Scientific Advisory Council of the non-profit Carbon Technology Research Foundation. M.V.M. is a member of the UK Government Defra Air Quality Expert Group. The remaining authors declare that they have no competing interests.

Additional information

Supplementary information The online version contains supplementary material available at https://doi.org/10.1038/s41612-024-00678-2.

Correspondence and requests for materials should be addressed to James Weber.